J Biomol NMR (2011) 50:1–11
DOI 10.1007/s10858-011-9496-2

COMMUNICATION

5D ^{13}C-detected experiments for backbone assignment of unstructured proteins with a very low signal dispersion

Jiří Nováček · Anna Zawadzka-Kazimierczuk · Veronika Papoušková · Lukáš Žídek · Hana Šanderová · Libor Krásný · Wiktor Koźmiński · Vladimír Sklenář

Received: 3 January 2011 / Accepted: 28 February 2011 / Published online: 20 March 2011

Abstract Two novel 5D NMR experiments (CACONCACO, NCOCANCO) for backbone assignment of disordered proteins are presented. The pulse sequences exploit relaxation properties of the unstructured proteins and combine the advantages of ^{13}C-direct detection, non-uniform sampling, and longitudinal relaxation optimization to maximize the achievable resolution and minimize the experimental time. The pulse sequences were successfully tested on the sample of partially disordered delta subunit from RNA polymerase from *Bacillus subtilis*. The unstructured part of this 20 kDa protein consists of 81 amino acids with frequent sequential repeats. A collection of 0.0003% of the data needed for a conventional experiment with linear sampling was sufficient to perform an unambiguous assignment of the disordered part of the protein from a single 5D spectrum.

Keywords Intrinsically disordered proteins · Non-uniform sampling · ^{13}C detection · Longitudinal relaxation optimization · Backbone assignment

Introduction

As much as 25–41% of the proteins in the eukaryotic genomes contain long regions that do not possess any regular secondary or tertiary structure (Dunker et al. 2000). Yet, these intrinsically disordered proteins (IDPs) fulfill a number of biological functions (Ward et al. 2004). NMR represents a method of choice for studies of unstructured proteins at atomic resolution as disordered systems are difficult to investigate using single-crystal X-ray diffraction. Already the backbone chemical shifts obtained in the process of sequential assignment are direct indicators of a residual secondary structure of IDPs (Eliezer 2007). Current state-of-the-art biomolecular NMR offers a variety of strategies for the backbone resonance assignment. The standard approach is based on the combination of triple-resonance experiments that provide the sequential information via (a) matching C^{α} and C^{β} chemical shifts, e.g. CBCA(CO)NH, HNCACB (Sattler et al. 1999; Pannetier et al. 2007; Rovnyak et al. 2004), or (b) correlating N chemical shifts, e.g. HNN, (H)CANNH or hNcaNH, hNcocaNH (Panchal et al. 2001; Zweckstetter et al. 2001; Frueh et al. 2006; Sun et al. 2005). A successful application of these experiments for the sequential assignment of IDPs has been reported in several cases (Pannetier et al. 2007; Peti et al. 2001; Yao et al. 2001; Mukrasch et al. 2009; Motáčková et al. 2009). However, the referred experiments may not provide sufficient resolving power for the unambiguous assignment of IDPs with a very high degeneracy of backbone chemical shifts. Especially in the

Electronic supplementary material The online version of this article (doi:10.1007/s10858-011-9496-2) contains supplementary material, which is available to authorized users.

J. Nováček · V. Papoušková · L. Žídek (✉) · V. Sklenář
Faculty of Science, NCBR, and CEITEC, Masaryk University, Kamenice 5, 625 00 Brno, Czech Republic
e-mail: lzidek@chemi.muni.cz

A. Zawadzka-Kazimierczuk · W. Koźmiński
Faculty of Chemistry, University of Warsaw, Pasteura 1, 02 093 Warsaw, Poland

H. Šanderová · L. Krásný
Laboratory of Molecular Genetics of Bacteria and Department of Bacteriology, Institute of Microbiology, Academy of Sciences of the Czech Republic, Vídeňská 1083, 142 20 Prague, Czech Republic

case of amino acid sequences with highly repetitive motifs, the assignment by standard biomolecular NMR methods fails due to severe signal overlaps. Recently, several highly sophisticated methods that use C^{α} and C^{β} chemical shifts or N and H^N shifts to provide a sequential connectivity in combination with high-dimensional experiments (5D or 7D) and automated data processing for the assignment of IDPs were described (Atreya et al. 2004, 2005; Hiller et al. 2005, 2007; Narayanan et al. 2010). Herein we present two novel 5D NMR experiments for the sequential assignment of IDPs featuring a severe signal overlap in conventional spectra. Their application allows backbone assignment from a single spectrum recorded in a time typical for a standard 3D experiment. The experiments have been successfully tested on a challenging biological system, the 20 kDa partially disordered δ-subunit of RNA polymerase unique for Gram-positive bacteria (BMRB 16912), where the sequential assignment using conventional methods completely failed (Motáčková et al. 2010b).

Materials and methods

Sample preparation, NMR experiments

The uniformly labeled [^{13}C, ^{15}N] δ-subunit was prepared as described earlier (Motáčková et al. 2010b). The final sample used for all the NMR measurements consisted of 0.8 mM δ-subunit, 20 mM phosphate buffer, pH 6.6, 10 mM NaCl, and 10% D_2O. All the experiments were performed at 301 K. The CACONCACO (Fig. 4) experiment was measured with the spectral widths set to 6,000 (aq) × 2,000 (^{15}N) × 3,125 ($^{13}C^{\alpha}$) Hz. The maximal evolution times in the indirectly detected dimensions were set to 24 ms for the $^{13}C^{\alpha}$ dimensions, to 50 ms for the ^{15}N dimension and to 32 ms for the $^{13}C'$ dimension. The experiment was measured in a pseudo 2D mode based on the parameter set for the standard 2D CACO with 8 transients per increment, and an interscan delay of 0.2 s. The NCOCANCO (Fig. 5) experiment was measured with the spectral widths set to 6,000 (aq) × 2,000 (^{15}N × 3,125 ($^{13}C^{\alpha}$) × 2,000 ($^{13}C'$) × 2,000 (^{15}N) Hz. The maximal evolutions in the indirectly detected dimensions were set to 32 ms for the ^{15}N dimensions, to 48 ms for the $^{13}C^{\alpha}$ dimension and to 9 ms for the $^{13}C'$ dimension. The data were acquired in a pseudo 2D mode based on the parameter set for the standard 2D CON experiment with 8 transients per increment, and an interscan delay of 0.2 s. Both experiments were recorded with 1,024 complex points in the acquisition dimension and 1,800 hypercomplex points were randomly distributed in the indirectly detected dimensions (see "Sampling scheme"). Auxiliary 3D (CACO)NCACO and (NCO)CANCO experiments were acquired using the proposed pulse sequences excluding the evolution of the chemical shift in t_1 and t_2. The (CACO)NCACO experiment was run with the following settings. Spectral widths were set to 6,000 (aq) × 3,125 ($^{13}C^{\alpha}$) × 2,000 (^{15}N) Hz. The maximal evolution times in the indirectly detected dimensions were set to 24 ms for the $^{13}C^{\alpha}$ dimension and to 50 ms for the ^{15}N dimension. The experiment was acquired with 8 scans per increment and a single scan recycling delay of 0.2 s. One thousand and twenty-four complex points were recorded in the acquisition dimension and the overall number of 900 hypercomplex points has been detected in the indirectly detected dimensions. The (NCO)CANCO experiment was acquired with the spectral widths set to 6,000 (aq) × 2,000 (^{15}N) × 3,125 ($^{13}C^{\alpha}$) Hz. The maximal evolution times in the indirectly detected dimensions were set to 32 ms for the ^{15}N dimension and to 48 ms for the $^{13}C^{\alpha}$ dimension. The data were recorded with 8 scans per increment and a single scan recycle delay of 0.2 s. The total number of 1,024 complex points was acquired in the directly detected dimension and 900 hypercomplex points were detected in indirect dimensions. The data were acquired on a 600 MHz Bruker Avance II spectrometer equipped with the first generation Bruker $^{1}H/^{13}C/^{15}N$ TCI cryogenic probehead with the z-axis gradients (S/N = 612 at the time of measurement in a standard ^{13}C sensitivity test on ASTM). In addition, the CACONCACO experiment was also measured on a 700 MHz Bruker Avance I spectrometer equipped with the Bruker $^{1}H/^{13}C/^{15}N$ TXO cryogenic probehead with the z-axis gradients dedicated for the ^{13}C-direct detection (S/N = 2,800 at the time of measurement in a standard ^{13}C sensitivity test on ASTM) with the spectral widths set to 10,600 (aq) × 5,000 ($^{13}C^{\alpha}$) × 3,125 (^{15}N) × 4,000 ($^{13}C'$) × 5,000 ($^{13}C^{\alpha}$) Hz. The maximal evolution times in the indirectly detected dimensions were set to 26 ms for the $^{13}C^{\alpha}$ dimensions, to 48 ms for the ^{15}N dimension and to 30 ms for the $^{13}C'$ dimension. The experiment was recorded with 4 transients per increment and an interscan delay of 0.3 s. The total number of 1,024 complex points was acquired in the directly detected dimension and 800 hypercomplex points were detected in the indirect dimensions.

Sampling scheme

Non-uniform sampling of the indirectly detected dimension was utilized in the presented application. The Poisson disc sampling scheme (Kazimierczuk et al. 2008), which introduces the distance constraints between the individual time points, was selected to generate the time schedule. Such a sampling scheme was shown to reduce the level of

sampling artifacts in the signal vicinity (Kazimierczuk et al. 2008). To create a sampling scheme, a new time point was randomly placed at the four-dimensional space, however, the minimal distance between the individual time points was defined. For that purpose, four-dimensional ellipsoids with the centres in each point present in the time schedule were created. The new point was accepted if its ellipsoid was not intersecting with any other ellipsoid, otherwise, the new point was rejected. If rejected, the different time point was randomly placed in the four-dimensional time space and the validation procedure was repeated. The individual radii of the ellipsoids created around the time point were set to:

$$a_1 = \frac{\alpha}{\sqrt[4]{8N}} \sqrt{\frac{\mathrm{SW}_2 \cdot t_2^{\max} \cdot \mathrm{SW}_3 \cdot t_3^{\max} \cdot \mathrm{SW}_4 \cdot t_4^{\max}}{(\mathrm{SW}_1 \cdot t_1^{\max})^3}} \quad (1)$$

$$a_2 = \frac{\alpha}{\sqrt[4]{8N}} \sqrt{\frac{\mathrm{SW}_1 \cdot t_1^{\max} \cdot \mathrm{SW}_3 \cdot t_3^{\max} \cdot \mathrm{SW}_4 \cdot t_4^{\max}}{(\mathrm{SW}_2 \cdot t_2^{\max})^3}} \quad (2)$$

$$a_3 = \frac{\alpha}{\sqrt[4]{8N}} \sqrt{\frac{\mathrm{SW}_1 \cdot t_1^{\max} \cdot \mathrm{SW}_2 \cdot t_2^{\max} \cdot \mathrm{SW}_4 \cdot t_4^{\max}}{(\mathrm{SW}_3 \cdot t_3^{\max})^3}} \quad (3)$$

$$a_4 = \frac{\alpha}{\sqrt[4]{8N}} \sqrt{\frac{\mathrm{SW}_1 \cdot t_1^{\max} \cdot \mathrm{SW}_2 \cdot t_2^{\max} \cdot \mathrm{SW}_3 \cdot t_3^{\max}}{(\mathrm{SW}_4 \cdot t_4^{\max})^3}}, \quad (4)$$

where α, N, SW_i, and $t_i^{\max}$ are: factor regulating the discrepancy of generated points ($\alpha = 0.8$), total number of generated time points, spectral width, and maximal evolution time for individual indirect dimensions, respectively. If the number of attempts to place the new point in the time space reached the relaxation condition T ($T = 5 \cdot N$), the individual radii of the ellipsoids were reduced (each radius was multiplied by a factor 0.9999) and the whole procedure was repeated until all points were generated. The overall number of $N = 1{,}800$ ($N = 800$ in the case of the data acquired at 700 MHz) points was placed in the four-dimensional time space. Finally, the constant density of the generated time points was transformed to the decaying density of points according to the Gaussian distribution ($\sigma = 0.5$).

Data processing

The 3D experiments were processed using Multidimensional Fourier Transform (MFT). Before applying MFT, the data were square cosine weighted, zero-filled to 2,048 points and transformed using the FFT algorithm in the directly detected dimension using spectral processing and analysis system NMRPipe/NMRDraw 3.0 (Delaglio et al. 1995). The number of spectral points was set to 1,536 in both indirectly detected dimensions. The non-uniformly sampled 5D data were processed using Sparse Multidimensional Fourier Transform algorithm (SMFT). The recorded data were square cosine weighted, zero-filled to 2,048 points, and transformed with the FFT algorithm in the directly detected dimension prior to SMFT. The number of spectral points was set to 512 in ω_1 and ω_2 ($\mathrm{C}^{\alpha}_{i-1}, \mathrm{C}'_{i-1}$ in the case of CA-CONCACO, and $\mathrm{N}_{i+1}, \mathrm{C}'_i$ in the case of NCOCANCO). All the spectra were analyzed in a graphical NMR assignment and integration software Sparky 3.115 (T.D. Goddard and D. G. Kneller, University of California, San Francisco, USA).

Results and discussion

The δ-subunit of the RNA-polymerase unique for Gram-positive bacteria is a 20 kDa partially unfolded protein that was shown to be important for the virulence of *Staphylococcus aureus* and *Streptococcus agalactiae* (Seepersaud et al. 2006). Although early studies of the δ-subunit can be tracked back to almost 30 years ago (Achberger et al. 1982), its function still remains unclear. In our previous study, we have determined the structure of the well ordered N-terminal domain of the δ-subunit from *Bacillus subtilis* (Motáčková et al. 2010a). Apart from the well ordered N-terminal region (91 amino acids), the full-length protein comprises a disordered C-terminal end (81 amino acids) that contains high incidence of sequential repeats in the primary structure. The sequential repeats cause severe clustering of the backbone chemical shifts, which makes the biologically relevant full-length δ-subunit a challenging sample for an NMR study. The poor chemical shift dispersion of nuclei employed in standard triple-resonance experiments used for sequential assignment (Sattler et al. 1999) is demonstrated in Fig. 1. Figure 1a and b show the clustering of the C^{α} and C^{β} chemical shifts, respectively. For example, two most frequently present amino acids in the sequence of the C-terminal region of the δ-subunit, aspartic acid (25 residues) and glutamic acid (23 residues), have their C^{α} and C^{β} chemical shifts distributed within 0.8 ppm (with 14 C^{β} chemical shifts in a range of 0.2 ppm), which makes the δ-subunit a very difficult target for assignment strategies based on C^{α} and C^{β} resonance frequencies. The comparison of the C^{α} and C^{β} chemical shift degeneracy of the δ-subunit and other proteins is depicted in Fig. 2. All the proteins described as disordered, unfolded, or unstructured in their BMRB entries, as well as two large structured proteins (malate synthase G and maltose binding protein), were used for that purpose. Figure 2 demonstrates that the δ-subunit exhibits one of the highest $\mathrm{C}^{\alpha}/\mathrm{C}^{\beta}$ chemical shift degeneracy among unstructured proteins studied so far. As a consequence, attempts to use the conventional assignment strategy based on matching the C^{α} and C^{β} chemical shifts in triple-resonance experiments completely failed for the δ-subunit. The data

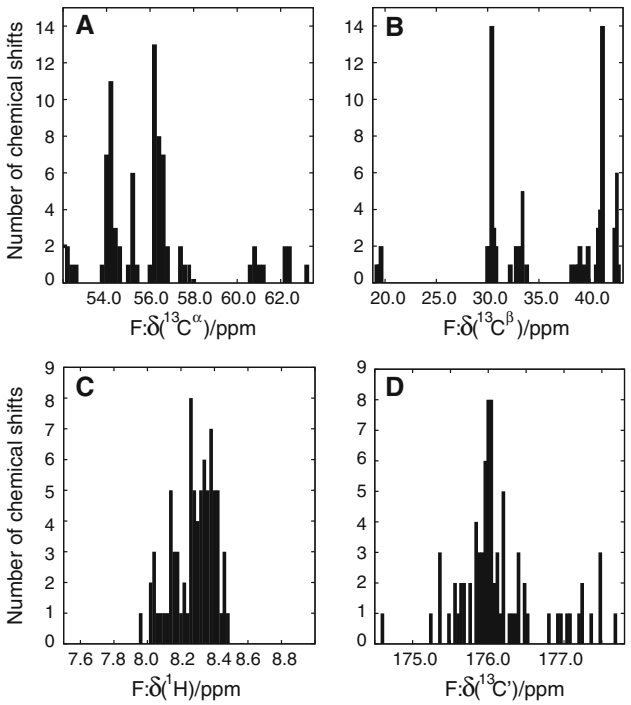

Fig. 1 Distribution of the chemical shifts of the disordered region of the δ-subunit. The bin size was set to 0.2 ppm for C^{α} (**a**) and C^{β} (**b**) chemical shifts. The bin size for H^N (**c**) and C′ (d) chemical shifts was set to 0.02 and 0.04 ppm, respectively

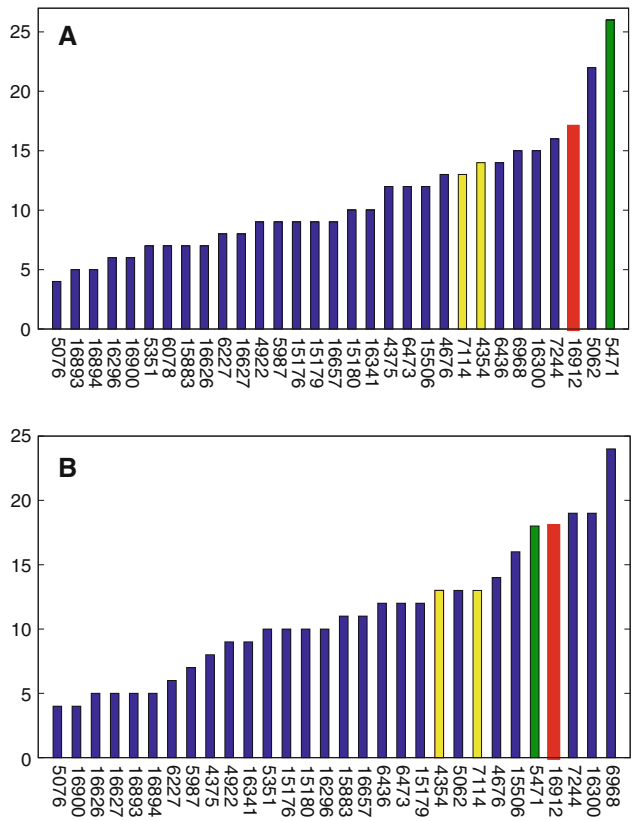

Fig. 2 Comparison of the C^{α} (**a**) and C^{β} (**b**) chemical shift degeneracy of the δ-subunit (*red*) with all proteins described as disordered, unfolded, or unstructured in their BMRB entries (*blue*), and with two large structured proteins, malate synthase G (723 residues, *green*) and maltose-binding protein (370 residues, *yellow*). Each column displays a maximal number of resonances observed within a 0.2 ppm chemical shift window for a given protein. The BMRB codes are indicated below the *bars*

used in the analysis shown in Figs. 1 and 2 was obtained in our previous study, where a set of 5D proton detected NMR experiments HN(CA)CONH and HabCabCONH, measured at a 700 MHz spectrometer, was utilized to perform the backbone assignment (Motáčková et al. 2010b). To make the process of the backbone assignment more efficient, we have designed two novel experiments that allow for the assignment of such a difficult system from a single 5D spectrum, providing thus all the relevant chemical shifts in one experiment and at identical conditions.

To overcome the degeneracy in the frequencies, four non-traditional tricks were combined in the experimental design. (a) The *direct* ^{13}C detection (Bermel et al. 2005, 2006a, 2006b; Knoblich et al. 2009; Perez et al. 2009) was employed to take advantage of the high dispersion of carbonyl signals (Fig. 1c, d). To allow for the direct comparison of the H^N and *C′* chemical shift dispersion, the graphs in Fig. 1c, d were plotted for the same range of resonance frequencies (500 Hz). The magnetogyric ratio for C′ and signal linewidth were used to scale the bin size for the C′ chemical shifts with respect to the H^N. Figure 1c and d clearly show a higher dispersion of the chemical shifts in the case of the direct C′ detection. (b) The resolution in the indirect dimensions was maximized by extending the maximal evolution times, taking advantage of relatively slow R_2 relaxation rates in IDPs. To accelerate the data collection, *non-uniform sampling* (NUS) was applied (Stern et al. 2002; Freeman et al. 2004; Orekhov et al. 2001; Marion 2006; Kazimierczuk et al. 2007; Malmodin and Billeter 2005; Mobli et al. 2008; Bretthorst, 2008). From available approaches, the Poisson disc sampling scheme (Kazimierczuk et al. 2008), which suppresses the level of sampling artefacts in a peak vicinity, was utilized. (c) *Five-dimensional* experimental arrangement empowered by implementation of NUS was found efficient to remove overlaps and ambiguities in the assignment procedure. (d) The methods for the *optimization of longitudinal relaxation* were employed to increase the acquisition rate and sensitivity of the measurements (Pervushin et al. 2002; Schanda et al. 2005; Bermel et al. 2009).

Although the applied ideas have already been described in the literature, their combination and the resulting benefits have not been reported yet. In order to quantify the

impact of the individual elements, three general parameters can be evaluated: relative *resolution*, given by product of chemical shift range and maximal evolution t^{max} time in each dimension; *sensitivity*, decaying exponentially with $-R_2 t^{max}$ in each (indirect) dimension; and overall *experimental time*, proportional to the number of increments. Using ^{13}C direct detection, the resolution in the directly detected dimension was increased 3.0 times compared to the scheme relying on amide proton detection in the case of the δ-subunit. The inherently lower sensitivity of direct ^{13}C detection is partially regained thanks to the favorable relaxation properties of ^{13}C at 600 or 700 MHz. Introduction of NUS to the indirect dimensions allows us to improve resolution by extending the maximal evolution times without increasing the number of increments until the limit of the natural linewidth is reached. Higher dimensionality offers another increase in resolution. In order to compare the effects of NUS and dimensionality, a simple comparison of 3D and 5D constant-time versions of a hypothetical experiment with identical R_2 and t^{max} for each dimension can be made. Higher sensitivity of the 3D version allows to acquire spectra with the same signal-to-noise ratio for the same number of increments with doubled lengths of the evolution periods of the 3D experiment compared to the 5D version. It corresponds to the four-fold enhancement in the resolution of the 3D version. On the other hand, the additional dimensions of the 5D experiment increase resolution by a factor of 100 (calculated for $1/t^{max} = 0.1 \times$ chemical shift range in each dimension). It shows that the effect of extending dimensionality is significantly higher. Resolution enhancement for the actual setting of the 5D experiments presented in this paper was ~200–500, compared to 3D versions of the experiments with similar t^{max} values. The major benefit of NUS is the reduction of the experimental time, necessary to perform the 5D experiments in practice. The 5D spectra recorded in this study were acquired in 0.02% (NCOCANCO at 600 MHz), 0.01% (CACONCACO at 600 MHz), and 0.0003% (CACONCACO at 700 MHz) of the theoretical durations of the corresponding uniformly sampled 5D experiments. A further two-fold to three-fold reduction of the measurement time was gained by the optimization of the longitudinal relaxation that allowed us to shorten the single scan recycle delay to 0.2–0.3 s. In summary, ~600–1,500-fold resolution enhancement was achieved without increasing the measurement time.

The most important improvement of the assignment efficiency was achieved by correlating C^{α}, C' or N, C' frequencies of neighboring residues instead of matching poorly dispersed C^{α}, C^{β} chemical shifts or correlating N, H^N frequencies (with lower dispersion of chemical shift of H^N compared to C'). Two novel 5D experiments, CACONCACO and NCOCANCO, providing such correlations and utilizing the elements listed above, were designed. Each of them is based on a different correlation with the distinct area of applications (*vide infra*). The magnetization transfer within the experiments is depicted in Fig. 3. The CACONCACO experiment exploits H^{α} as a starting point of magnetization transfer and correlates frequencies of $C^{\alpha}_{i-1}, C'_{i-1}, N_i, C^{\alpha}_i$, and C'_i (Fig. 3a). The sequential information is contained in the C^{α} and C' chemical shifts. The NCOCANCO experiment starts from H^N and carries information on $N_{i+1}, C'_i, C^{\alpha}_i, N_i$, and C'_{i-1} chemical shifts (Fig. 3b). The sequential connectivity is contained in the C' and N chemical shifts. The described scheme makes CACONCACO the experiment of choice in the case of proline rich proteins or in spectra with a good dispersion of C^{α} signals. The second experiment, NCOCANCO, is preferable when measuring deuterated proteins or in the case of spectra with high N signal dispersion. The pulse sequences for CACONCACO and NCOCANCO are depicted in Figs. 4 and 5, respectively. Although the chemical shift of ^1H is not measured in any of the experiments, the ^1H polarization was chosen as a starting point for magnetization transfer to maximize the sensitivity. A refocused INEPT transfer step referred to as "H-flip" (Bermel et al. 2009) was implemented in the case of CACONCACO for the enhancement of the longitudinal relaxation (Pervushin et al. 2002). Bipolar gradients (Sklenář 1995) were added to avoid radiation damping. H^N selective pulses were employed in the NCOCANCO experiment for the same purpose (Schanda et al. 2005). To further maximize the sensitivity, the magnetization transfer through the $^2J(NC^{\alpha})$ coupling was suppressed (Brutscher 2002; Fiotito et al. 2006). The suppression of the back transfer of magnetization is performed during the period denoted as t_3 in Figs. 4 and 5. The Cartesian product

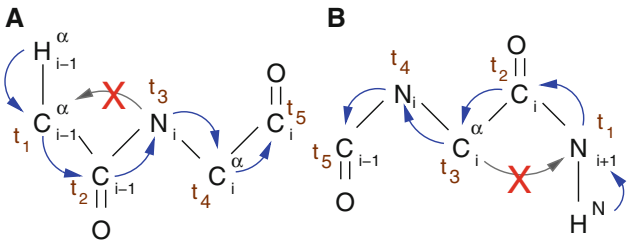

Fig. 3 Magnetization transfer in the CACONCACO (**a**) and NCOCANCO (**c**) experiments (*blue arrows*). The *back transfer* of magnetization (*grey arrow*) via $^2J(NC^{\alpha})$ is actively suppressed within the pulse sequences. The evolution times in the individual detected dimensions are indicated in *brown*. The maximal evolution times in indirect dimensions of the constant-time versions of experiments can be stretched to $t_1^{max} = 27.0$ ms, $t_2^{max} = 32.0$ ms, $t_3^{max} = 50.0$ ms, $t_4^{max} = 27.0$ ms (CACONCACO) and to $t_1^{max} = 32.0$ ms, $t_2^{max} = 9.0$ ms, $t_3^{max} = 54.0$ ms, $t_4^{max} = 32.0$ ms (NCOCANCO)

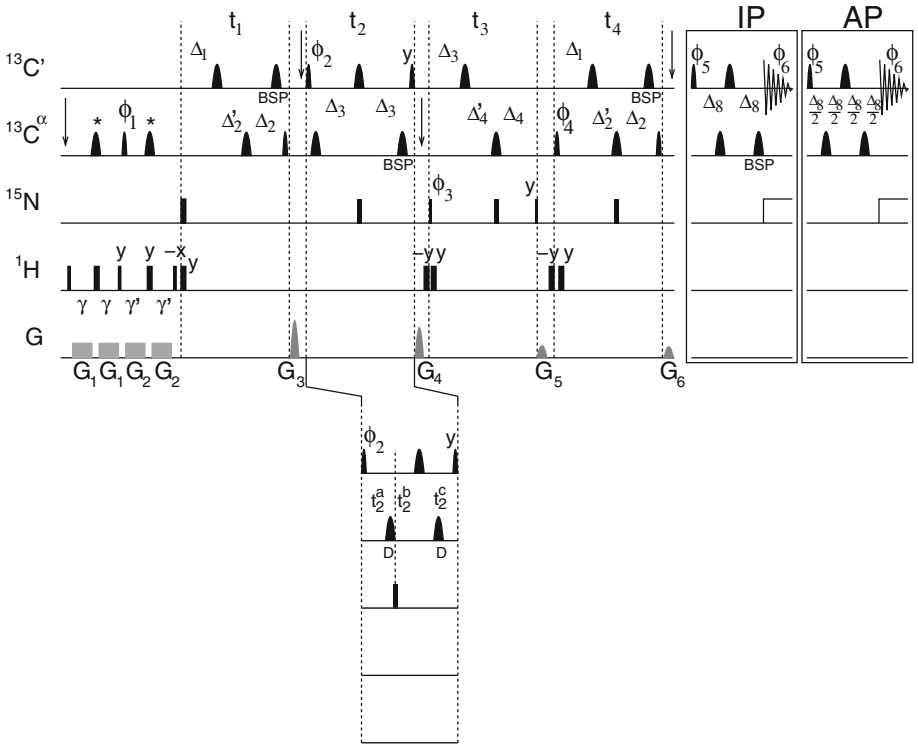

Fig. 4 Pulse scheme of 5D CACONCACO experiment. The carrier frequencies were placed at 4.7 ppm for ^{1}H, at 123.0 ppm for ^{15}N, and at 175.0 ppm for ^{13}C′, or 58.0 ppm for ^{13}C$^{\alpha}$. The *arrows* indicate the switching of the ^{13}C carrier frequency. *Narrow* and *wide symbols* stand for 90° and 180° pulses, respectively. The pulses were applied with the *x* phase unless noted differently. The *rectangles* represent non-selective pulses, whereas the round shapes represent selective pulses. The 320 μs 90° Q5 (or time-reversed Q5) and 256 μs 180° Q3 were used for ^{13}C′ and ^{13}C$^{\alpha}$/^{13}C$^{\mathrm{ali}}$ excitation resp. inversion at 600 MHz. 1,000 μs Q3 (denoted with *asterisk*) were used for selective inversion of ^{13}C$^{\alpha}$ with respect to ^{13}C$^{\beta}$. BSP denotes pulses for compensation of the off-resonance effects. The IPAP acquisition scheme was implemented to avoid signal splitting due to the ^{13}C$^{\alpha}$–^{13}C′ coupling. The *line denoted with G* stands for pulsed field gradients applied along the *z*-axis. G_1 (1,750 μs) and G_2 (1050 μs) are rectangular 1.2 G/cm pulses shape whereas the rest of the gradient pulses is of a sine-bell shape (1,000 μs). The GARP4 pulse train was used during the acquisition for ^{15}N decoupling. The following phase cycling was employed: $\phi_3 = x, \ -x$; $\phi_4 = 2(x), 2(-x)$; $\phi_{5\mathrm{IP}} = 4(x), 4(-x)$; $\phi_{5\mathrm{AP}} = 4(y), 4(-y)$; $\phi_6 = x, 2(-x), x, \ -x, 2(x), x$. The initial lengths of the delays were: $\gamma = 1.8\,\mathrm{ms}, \gamma' = 1.1\,\mathrm{ms}, \Delta_1 = 4.5\ \mathrm{ms}, \Delta_2 = 13.5\ \mathrm{ms}, \Delta_3 = 16.0\ \mathrm{ms}, \Delta_4 = 25.0\,\mathrm{ms}, \Delta_8 = 4.5\,\mathrm{ms}, \Delta_2' = \Delta_2 - \Delta_1, \Delta_4' = \Delta_4 - \Delta_3$. The constant-time mode of chemical shift evolution was implemented in all indirect evolution periods (t_1, t_2, t_3, t_4). The evolution of the chemical shift can be switched to the semi-constant time mode to further increase the resolution in resulting spectra when necessary. The building block for evolution of the chemical shift in semi-constant time mode is indicated below the diagram. The *pulses denoted with "D"* were continuously centred with respect to $t_2^{\mathrm{a}} + t_2^{\mathrm{b}}$, and t_2^{c} delays. The initial length of the incremented delays were set to: $t_2^{\mathrm{a}}(0) = 16.0\,\mathrm{ms}$, $t_2^{\mathrm{b}}(0) = 0.0\,\mathrm{ms}$, and $t_2^{\mathrm{c}}(0) = 16.0\,\mathrm{ms}$ and the increments were adjusted to $\Delta t_2^{\mathrm{a}} = 1/2\mathrm{SW}_2, \Delta t_2^{\mathrm{c}} = -t_2^{\mathrm{c}}(0)/\mathrm{TD}_2, \Delta t_2^{\mathrm{b}} = t_2^{\mathrm{a}} - t_2^{\mathrm{c}}$, where the SW and TD denote spectral width and number of complex points acquired in given indirect dimension in the case of uniform sampling, respectively. Quadrature detection in the indirect dimensions was achieved by incrementing phases ϕ_1, ϕ_2, ϕ_3, ϕ_4 in a States manner

operators (Sørensen et al. 1984) at the beginnings of the t_3 periods are given by $\mathrm{N}_i^z\mathrm{C}'^z_{i-1}\mathrm{C}_i^{\alpha,z}$ and $C_i^{\alpha,z}C_i'^zN_{i+1}^z$ for CACONCACO and NCOCANCO (Fig. 3), respectively. Both $^{1}J(\mathrm{NC}^{\alpha})$ and $^{2}J(\mathrm{NC}^{\alpha})$ scalar couplings are active during this period (as well as the $J(\mathrm{NC}')$ coupling employed to refocus the carbonyl magnetization), and lead to the evolution of operators $\mathrm{N}_i^z\mathrm{C}_i^{\alpha,z}$ for the desired transfer of magnetization and $\mathrm{N}_i^z\mathrm{C}_{i-1}^{\alpha,z}$ for the suppressed transfer in the case of CACONCACO, and to the evolution of $\mathrm{C}_i^{\alpha,z}\mathrm{N}_i^z$ for the desired transfer and $\mathrm{C}_i^{\alpha,z}\mathrm{N}_{i+1}^z$ for the suppressed transfer of magnetization in the case of NCOCANCO at the end of t_3 period. The transfer amplitudes for the states described by the individual operators are given by:

$$\mathrm{N}_i^z\mathrm{C}_i^{\alpha,z} : \sin(\pi \cdot {}^{1}J(\mathrm{NC}^{\alpha}) \cdot t_3) \times \sin(\pi \cdot {}^{2}J(\mathrm{NC}^{\alpha}) \cdot t_3) \quad (5)$$

$$\mathrm{N}_i^z\mathrm{C}_{i-1}^{\alpha,z} : \cos(\pi \cdot {}^{1}J(\mathrm{NC}^{\alpha}) \cdot t_3) \times \cos(\pi \cdot {}^{2}J(\mathrm{NC}^{\alpha}) \cdot t_3) \quad (6)$$

$$\mathrm{C}_i^{\alpha,z}\mathrm{N}_i^z : \sin(\pi \cdot {}^{1}J(\mathrm{NC}^{\alpha}) \cdot t_3) \times \sin(\pi \cdot {}^{2}J(\mathrm{NC}^{\alpha}) \cdot t_3) \times \cos(\pi \cdot J(\mathrm{C}^{\alpha}\mathrm{C}^{\beta}) \cdot t_3) \quad (7)$$

$$\mathrm{C}_i^{\alpha,z}\mathrm{N}_{i+1}^z : \cos(\pi \cdot {}^{1}J(\mathrm{NC}^{\alpha}) \cdot t_3) \times \cos(\pi \cdot {}^{2}J(\mathrm{NC}^{\alpha}) \cdot t_3) \times \cos(\pi \cdot J(\mathrm{C}^{\alpha}\mathrm{C}^{\beta}) \cdot t_3). \quad (8)$$

Transfer efficiencies of the operators described by Eqs. (5, 6), and (7, 8) are plotted in Fig. 6a, b, respectively. The values of $t_3 = 50$ ms in the case of CACONCACO, and $t_3 = 54$ ms in the case of NCOCANCO experiment were found optimal to minimize the transfer of magnetization

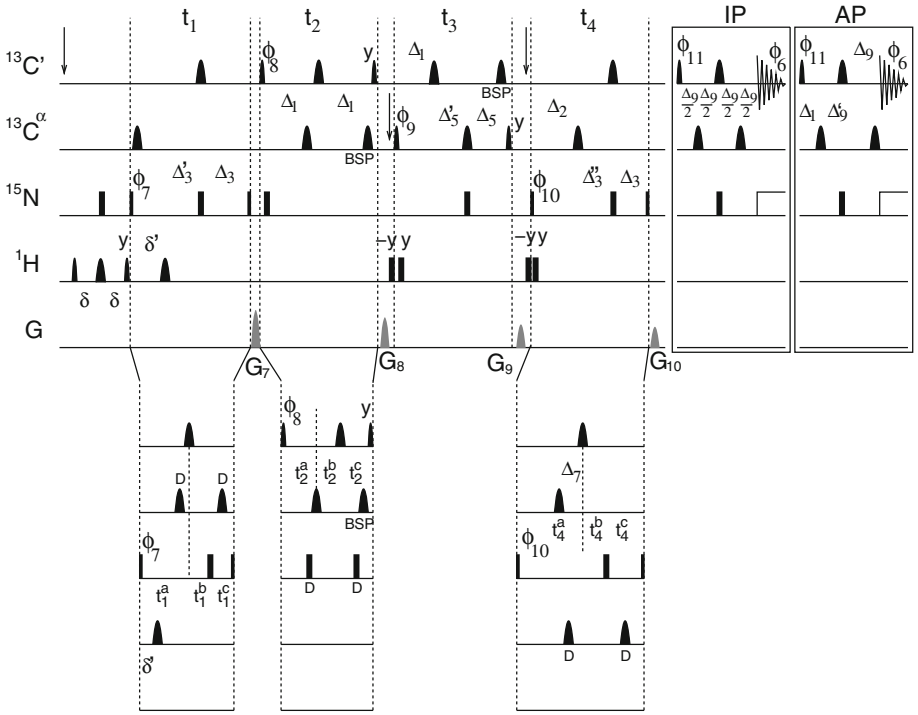

Fig. 5 Pulse sequence of 5D NCOCANCO experiment. The carrier frequencies for the hard and shaped ^{1}H pulses were placed at 4.7 and 8.2 ppm, respectively. The carriers for ^{15}N were placed at 123.0 ppm, and at 175.0 ppm for ^{13}C′, or at 58.0 ppm for ^{13}C$^{\alpha}$. The *arrows* indicate the switching of the ^{13}C carrier frequency. *Narrow* and *wide symbols* stand for 90° and 180° pulses, respectively. The pulses were applied with the *x* phase unless noted differently. The *rectangles* represent ^{15}N and ^{1}H non-selective pulses, the *round shapes* represent selective ^{1}H and ^{13}C pulses. The 90° E-burp pulses of the length of 1,600 μs (the first one applied in time-reversed mode) and 180° RE-burp pulses of the length of 1,700 μs were applied for selective excitation resp. inversion of ^{1}H^{N}. The 320 μs 90° Q5 (or time-reversed Q5) and 256 μs 180° Q3 were used for ^{13}C′ and ^{13}C$^{\alpha}$/^{13}C^{ali} excitation resp. inversion at 600 MHz. BSP denotes pulses for compensation of the off-resonance effects. The IPAP acquisition scheme was implemented to avoid signal splitting due to the ^{13}C$^{\alpha}$–^{13}C′ coupling. The *line denoted with G* stands for pulsed field gradients applied along the *z*-axis. All gradient pulses are of a *sine-bell shape* of the length of 1,000 μs. The GARP4 pulse train was used during the acquisition for ^{15}N decoupling. The following phase cycling was employed: $\phi_7 = x, -x;\ \phi_8 = 2(x), 2(-x);\ \phi_{11IP} = 4(x), 4(-x);\ \phi_{11AP} = 4(-y), 4(y);\ \phi_6 = x, 2(-x), x, -x, 2(x), x$. The initial lengths of the delays were: $\delta = 395\ \mu s, \delta' = 1.876$ ms, $\Delta_1 = 4.5$ ms, $\Delta_2 = 13.5$ ms, $\Delta_3 = 16.0$ ms, $\Delta_5 = 27.0$ ms, $\Delta_9 = 16.0$ ms, $\Delta'_3 = \Delta_3 - \delta', \Delta'_5 = \Delta_5 - \Delta_1, \Delta''_3 = \Delta'_3 - \Delta_2, \Delta'_9 = \Delta_9 - \Delta_1$. The constant time mode of the evolution of chemical shift was used in all indirect evolution period (t_1, t_2, t_3, t_4). The evolution of the chemical shift can be switched to the semi-constant time mode to further increase the resolution in resulting spectra when necessary. The building blocks the semi-constant time mode are indicated below the *diagram*. The *pulses denoted with "D"* were continuously centred with respect to $t_1^a + t_1^b, t_2^a + t_2^b, t_4^a + t_4^b, t_1^c, t_2^c$, and t_4^c delays. The δ' was initially set to 1.876 ms and continuously adjusted to completely refocus the ^{1}H^{N}-^{15}N coupling. The initial length of the incremented delays were set to: $t_1^a(0) = t_1^c(0) = 16.0$ ms, $t_2^a(0) = t_2^c(0) = 4.5$ ms, $t_4^a(0) = 13.5$ ms, $t_4^c(0) = 16.0$ ms, $t_1^b(0) = t_2^b(0) = t_4^b(0) = 0.0$ ms, $\Delta_7 = t_4^c(0) - t_4^a(0)$, and the increments were adjusted to $\Delta t_{1,2,4}^a = 1/2SW_{1,2,4}, \Delta t_{1,2,4}^c = -t_{1,2,4}^c(0)/TD_{1,2,4}, \Delta t_{1,2,4}^b = t_{1,2,4}^a - t_{1,2,4}^c$, where SW_i and TD_i denotes spectral width and number of complex points acquired in given dimension in the case of uniform sampling, respectively. Quadrature detection in the indirect dimensions was achieved by incrementing phases ϕ_7, ϕ_8, ϕ_9, ϕ_{10} in a States manner

via ^{2}J(NC$^{\alpha}$) coupling and maximize the sensitivity of the experiments.

To retrieve the frequency information from the 5D data, a set of reduced dimensionality spectra can be recorded and coupled with the automated data analysis (Atreya et al. 2004; Hiller et al. 2005; Narayanan et al. 2010), or techniques to recover the spectrum of full dimensionality (Kazimierczuk et al. 2010; Zawadzka-Kazimierczuk et al. 2010) can be employed. The latter approach was utilized in the presented application due to its similarity to the handling of standard 2D and 3D spectra. As processing of 5D data to a full 5D spectrum would demand terabytes of disc space, only 2D cross sections of the 5D matrix were calculated using the Sparse Multidimensional Fourier Transform (SMFT) algorithm (Kazimierczuk et al. 2009). First, three-dimensional versions of the proposed experiments correlating N_i, C_i^{α}, C_i' in the case of CACONCACO (Fig. 3a) and C_i^{α}, N_i, and C'_{i-1} in the case of NCOCANCO (Fig. 3b) were measured and signals were identified in the obtained 3D spectra. Then, 2D cross sections ($C_{i-1}^{\alpha}, C'_{i-1}$ in the case of CACONCACO and N_{i+1}, C_i' in the case of NCOCANCO) from the 5D data that carry the sequential information were calculated for each triplet of frequencies measured in the 3D experiment. The resulting spectra are

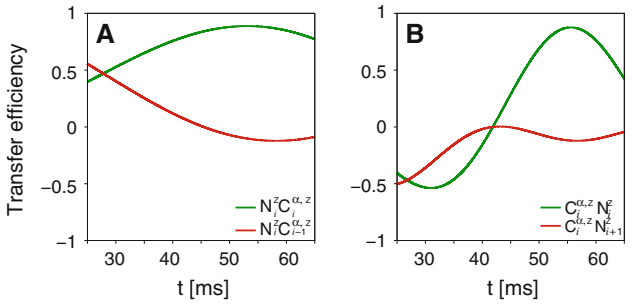

Fig. 6 Plots of transfer amplitudes defining transfer efficiencies of the operators in Eqs. (5, 6) (**a**), and Eqs. (7, 8) (**b**). The values of $^1J(\mathrm{NC}^\alpha) = 11.0$ Hz, $^2J(\mathrm{NC}^\alpha) = 7.0$ Hz, $J(\mathrm{C}^\alpha\mathrm{C}^\beta) = 35.0$ Hz (Sattler et al. 1999) have been used for the purpose of plotting the graphs

very simple and offer direct interpretation. Such spectra are well suited for automated peak-picking and analysis. Nevertheless, the manual assignment was prioritized in the presented application. This approach allows visual inspection of the problematic regions in the spectra as well as eventual corrections in the peak picking. The manual assignment procedure for the NCOCANCO experiment is outlined in Fig. 7. The position of the kth peak (cyan) selected in the auxiliary 3D spectrum (a) is given by frequencies $\omega_3^k, \omega_4^k, \omega_5^k$ corresponding to the chemical shifts of the C_i^α, N_i, and C'_{i-1}, highlighted in the 3D peak list (b). A 2D cross-section of the 5D spectrum is calculated for these three frequencies (c). Frequencies ω_1^k, ω_2^k of the peak observed in the 2D cross section (d) provide chemical shifts of N_{i+1} and C'_i from the following residue. In the next step, a column at $\omega_4^{k+1} = \omega_1^k, \omega_5^{k+1} = \omega_2^k$, containing the violet $(k+1)$th peak, is selected in the 3D spectrum. The next 2D cross-section is then calculated for the frequencies $\omega_3^{k+1}, \omega_4^{k+1}, \omega_5^{k+1}$ of the violet peak and the whole procedure is repeated. The assignment protocol for the CACONCACO experiment is analogous but it proceeds in the opposite direction, i.e., the preceding residue is defined in each step.

The resolution enhancement in the measured 5D spectra is demonstrated in Fig. 8, comparing 2D cross-section of 5D NUS NCOCANCO, and a plane from a uniformly sampled 3D HNCO. It should be noted that the maximal evolution time of the C′ dimension of the 2D cross-section displayed in Fig. 8 (right) was the shortest one of those used in this study. Two examples of the 2D cross sections for the NCOCANCO experiment are shown in Fig. 9a, b. The spectrum in Fig. 9a contains a single peak that gives the sequential connectivity directly. Note that such unambiguous assignment (based on N, C′ correlations) was obtained for two residues in a stretch of four glutamates (E168-E171), which C^α and C^β chemical shifts are in the range of 56.434–56.602 and 30.205–30.519 ppm, respectively. The spectrum in Fig. 9b contains two peaks

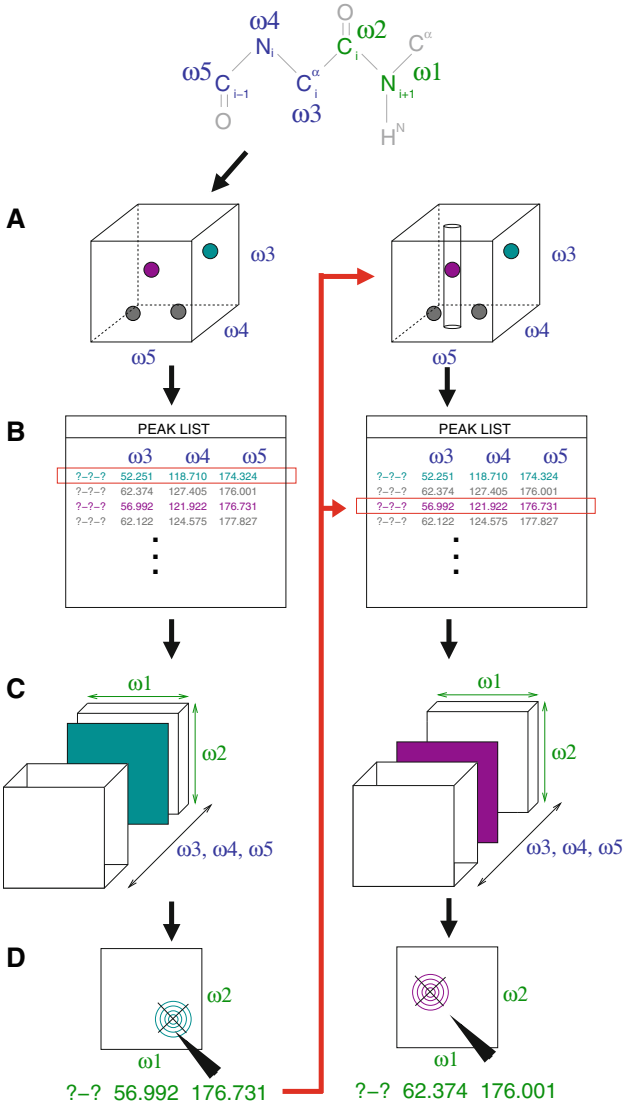

Fig. 7 Schematic diagram of the processing and manual assignment procedure for the 5D data

indicating that $\mathrm{C}_i^\alpha, \mathrm{N}_i, \mathrm{C}'_{i-1}$ frequencies of two amino acids are almost identical and cannot be resolved in the 3D experiment (Fig. 9c). Thanks to the gain in resolution given by additional two frequencies, such problematic regions can be resolved in the 5D spectrum (Fig. 9b). Subsequently, two possible routes are followed in the assignment protocol (Fig. 7) until one of them is ruled out.

One hundred percentage of the ^{13}C and ^{15}N backbone chemical shifts of the 81 amino acid long disordered part of the protein were assigned by each experiment. The time needed to perform the manual assignment did not exceed 24 working hours. The correctness of the assignment obtained from a single spectrum (either NCOCANCO or CACONCACO) was confirmed by a comparison with the assignment derived from a combination of ^{1}H-detected 5D HN(CA)CONH and HabCabCONH spectra recorded at the

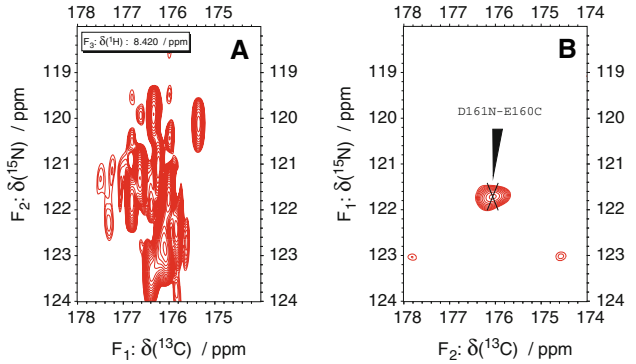

Fig. 8 Plane from a uniformly sampled 3D HNCO spectrum at $\delta(^1H) = 8.42$ ppm showing the region of the spectrum containing the resonance signal of D161N-E160C (*left*), and 2D cross-section from 5D NCOCANCO experiment calculated showing the D161N-E160C resonance signal (*right*). The contour threshold was set to 40% of the selected peak height

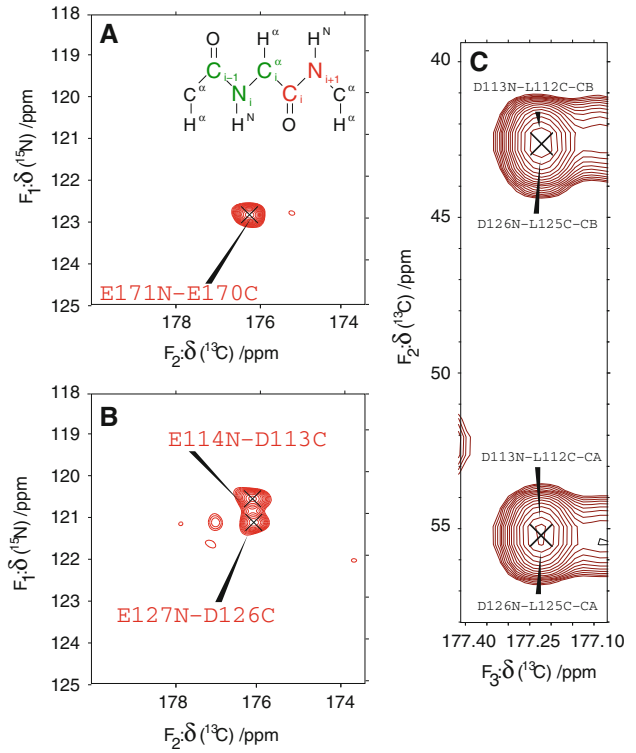

Fig. 9 2D cross-sections from the 5D NCOCANCO experiment (**a**, **b**; *inset* in *panel A* applies to both panels) showing sequential connectivity peaks for the frequencies (*marked green*) of E170CA-N-E169C (**a**), D113CA-N-L112C, and D126CA-N-L125C (**b**). The strip from NUS 3D ^{13}C detected CBCACON experiment at ^{15}N frequency 121.059 ppm (**c**)

700 MHz spectrometer (Motáčková et al. 2010b). The data acquisition on the 600 MHz spectrometer with the first generation cryoprobe took 60 h per experiment, which constitutes less than 0.02% of time needed for a conventional experiment with linear sampling using similar settings. The acquisition of the CACONCACO experiment on the 700 MHz spectrometer with a state-of-the-art probe providing 4.5 times higher sensitivity for direct ^{13}C detection took 14.5 h, which covers 0.0003% of time of the conventional experiment with similar settings.

The described assignment method should be compared to the recently published state-of-the-art approaches. A direct comparison to our recent work (Motáčková et al. 2010b) is possible as identical samples were used and data acquired at the same magnetic field are available. In both cases, a complete backbone assignment of the disordered highly repetitive C-terminal domain was achieved. Using pulse sequences presented in this article, we were able to obtain data needed for the complete assignment with comparable signal-to-noise ratio from one experiment in one third of the time of the experiments reported previously (Motáčková et al. 2010b). This demonstrates that the pulse sequences described in this paper can save the overall experimental time in spite of the inherently lower sensitivity of ^{13}C detection. However, the major progress of the approach presented here is a dramatic simplification of the assignment procedure. The proton-detected 5D HN(CA)-CONH spectrum (Motáčková et al. 2010b) allowed us to find sequential connectivities for 10 short fragments of the sequence. The 5D HabCabCONH spectrum was then used to classify residue types in the fragments (based on typical H^{α}, H^{β}, C^{α}, C^{β} chemical shifts) and thus to identify positions of the fragments in the amino acid sequence. On the contrary, the assignment procedure described in this paper (Fig. 7) provided sequential assignment from a single spectrum (CACONCACO or NCOCANCO) in a straightforward manner and therefore in a much shorter time needed to complete the analysis. A full set of 2D cross-sections of the 5D CACONCACO experiment shown in Fig. S1 of Supplementary Material documents the efficiency of the described assignment protocol. In addition, the fact that all chemical shifts are derived from one spectrum guarantees that all frequencies are measured at identical conditions. It may be particularly important in the case of highly repetitive IDP sequences, where e.g. minor temperature differences originating from nonidentical sample heating of individual experiments may complicate the identification of chemical shifts showing extremely low dispersion.

Automatic assignment of 93% non-proline and 83% total amino acids of the 441-residue protein Tau (Narayanan et al. 2010) from 7D HNCO(CA)CBCANH and 5D HACACONH APSY (Hiller et al. 2005, 2007) spectra represents another recent approach that should be discussed in the context of this study. The 2.5 fold difference in the size of the assigned proteins does not allow to compare the performance of the approaches directly. The higher (100%) percentage of assigned residues and shorter measurement

time (14.5 h at 700 MHz vs. 60 h at 900 MHz) of our approach can be at least partially attributed to the smaller size of the δ-subunit. On the other hand, the published spectra of protein Tau (Narayanan et al. 2010; Mukrasch et al. 2009) exhibit better chemical shift dispersion than the spectra of the δ-subunit (Motáčková et al. 2010b). Nevertheless, the comparison of these studies shows that both strategies can be considered complementary, our approach being well suited for smaller proteins with extremely low signal dispersion. For such applications, the presented pulse sequences provide several benefits: (a) The 5D CACONCACO experiment allows to determine sequential connectivity for proline residues. (b) Avoiding magnetization transfer via amide protons makes the 5D CACONCACO experiment beneficial for studies of systems at high pH. (c) While the 7D APSY relies on the correlation of N, H^N frequencies, our experiments exploit N, C′ or $C^{\alpha}C'$ correlations with higher resolution given by the higher dispersion of the C′ chemical shifts. (d) The manual interpretation of our 5D spectra is very simple and provides additional transparency and flexibility over the automated protocols as spectral regions with potential overlaps can be visually inspected and peak picking can be manually corrected if needed.

Conclusions

In conclusion, we have presented an approach for the unambiguous assignment of IDPs with high degeneracy in the amino acid sequence from a single 5D spectrum that maximizes the resolution and minimizes the experimental time. To our knowledge, this is the first application of direct ^{13}C detection to an experiment with dimensionality higher than three. The sequential connectivity is encoded in C', N or C', C^{α} frequencies rather than in C^{α}, C^{β} or N, H^N chemical shifts, which reduces the probability of an ambiguous assignment. Moreover, each experiment provides two chemical shifts (C', C^{α}) that are commonly used to assess the residual secondary structure content of the IDPs (results for the δ-subunit will be published elsewhere). Our results demonstrate that, despite the inherently lower sensitivity of ^{13}C detection, a complete assignment of an IDP with high degeneracy in primary sequence can be easily obtained even on a low field magnet (600 MHz) equipped with a relatively old cryogenic probe (see "Materials and methods").

Acknowledgements This work was supported by the Grants of the Ministry of Education of Czech Republic MSM0021622413 and LC06030, by the Grants 204/09/0583, 301/09/H004 and P206/11/0758 from Czech Science Foundation, by the EU/ grant POSTBIOMIN (FP7-REGPOT-2007-1 No. 205872), by MPD program from Foundation for Polish Sciences that was co-financed by the European Regional Development Fund. Financial support including the form of Access to the Bio-NMR Research Infrastructure co-funded under the 7th Framework Programme of the EC (FP7/2007-2013) grant agreement 261863 for conducting the research is gratefully acknowledged.

References

Achberger EC, Hilton MD, Whiteley HR (1982) The effect of the delta subunit on the interaction of *Bacillus subtilis* RNA polymerase with bases in a SP82 early gene promoter. Nucl Acids Res 10:2893–2910

Atreya HS, Szyperski T (2004) G-matrix Fourier transform NMR spectroscopy for complete protein resonance assignment. PNAS 101(26):9642–9647

Atreya H, Eletsky A, Szyperski T (2005) Resonance assignment of proteins with high shift degeneracy based on 5D spectral information encoded in G(2)FT NMR experiments. J Am Chem Soc 127(13):4554–4555

Bermel W, Bertini I, Duma L, Felli IC, Emsley L, Pierattelli R, Vasos PR (2005) Complete assignment of heteronuclear protein resonances by protonless NMR spectroscopy. Angew Chem Int Ed 44(20): 3089–3092

Bermel W, Bertini I, Felli IC, Piccioli M, Pierattelli R (2006) C-13-detected protonless NMR spectroscopy of proteins in solution. Prog Nucl Magn Reson Spectrosc 48(1):25–45

Bermel W, Bertini I, Felli I, Lee Y, Luchinat C, Pierattelli R (2006) Protonless NMR experiments for sequence-specific assignment of backbone nuclei in unfolded proteins. J Am Chem Soc 128 (12):3918–3919

Bermel W, Bertini I, Felli IC, Piccioli M, Pierattelli R (2009) Speeding up C-13 direct detection biomolecular NMR spectroscopy. J Am Chem Soc 131(42):15339–15345

Bretthorst GL (2008) Nonuniform sampling: bandwidth and aliasing. Concepts Magn Reson 32A(6):417–435

Brutscher B (2002) Intraresidue HNCA and COHNCA experiments for protein backbone resonance assignment. J Magn Reson 156(1):155–159

Delaglio F, Grzesiek S, Vuister G, Zhu G, Pfeifer J, Bax A (1995) NMRPipe: a multidimensional spectral processing system based on UNIX pipes. J Biomol NMR 6(3):277–293

Dunker AK, Obradovic Z, Romero P, Garner EC, Brown CJ (2000) Intrinsic protein disorder in complete genomes. Genome Inform 11:161–171

Eliezer D (2007) Characterizing residual structure in disordered protein states using nuclear magnetic resonance. Methods Mol Biol 350:49–67

Fiorito F, Hiller S, Wider G, Wüthrich K (2006) Automated resonance assignment of proteins: 6D APSY-NMR. J Biomol NMR 35(1):27–37

Freeman R, Kupče E (2004) Distant echoes of the accordion: reduced dimensionality, GFT-NMR, and projection-reconstruction of multidimensional spectra. Concepts Mang Reson 23(2):63–75

Frueh DP, Sun ZYJ, Vosburg DA, Walsh CT, Hoch JC, Wagner G (2006) Non-uniformly sampled double-TROSY hNcaNH experiments for NMR sequential assignments of large proteins. J Am Chem Soc 128(17):5757–5763

Hiller S, Fiorito F, Wuthrich K, Wider G (2005) Automated projection spectroscopy (APSY). PNAS 102(31):10876–10881

Hiller S, Wasmer C, Wider G, Wüthrich K (2007) Sequence-specific resonance assignment of soluble nonglobular proteins by 7D APSY-NMR spectroscopy. J Am Chem Soc 129(35):10823–10828

Kazimierczuk K, Zawadzka A, Koźmiński W, Zhukov I (2007) Lineshapes and artifacts in Multidimensional Fourier Transform of arbitrary sampled NMR data sets. J Magn Reson 188(2): 344–356

Kazimierczuk K, Zawadzka A, Koźmiński W (2008) Optimization of random time domain sampling in multidimensional NMR. J Magn Reson 192(1):123–130

Kazimierczuk K, Zawadzka A, Koźmiński W (2009) Narrow peaks and high dimensionalities: exploiting the advantages of random sampling. J Magn Reson 205(2):286–292

Kazimierczuk K, Zawadzka-Kazimierczuk A, Koźmiński W (2010) Non-uniform frequency domain for optimal exploitation of non-uniform sampling. J Magn Reson 197(2):219–228

Knoblich K, Whittaker S, Ludwig C, Michiels P, Jiang T, Schaffhausen B, Guenther U (2009) Backbone assignment of the N-terminal polyomavirus large T antigen. Biomol NMR Assign 3(1):119–123

Malmodin D, Billeter M (2005) Multiway decomposition of NMR spectra with coupled evolution periods. J Am Chem Soc 127 (39):13486–13487

Marion D (2006) Processing of ND NMR spectra sampled in polar coordinates: a simple Fourier transform instead of a reconstruction. J Biomol NMR 36(1):45–54

Mobli M, Hoch JC (2008) Maximum entropy spectral reconstruction of nonuniformly sampled data. Concepts Magn Reson 32A(6): 436–448

Motáčková V, Kubíčková M, Kožíšek M, Grantz-Šašková K, Švec M, Žídek L, Sklenář V (2009) Backbone H-1, C-13, and N-15 NMR assignment for the inactive form of the retroviral protease of the murine intracisternal A-type particle, inMIA-14 PR. Biomol NMR Assign 3(2):261–264

Motáčková V, Šanderová H, Žídek L, Nováček J, Padrta P, Švenková A, Korelusová J, Jonák J, Krásný L, Sklenář V (2010) Solution structure of the N-terminal domain of *Bacillus subtilis* delta subunit of RNA polymerase and its classification based on structural homologs. Proteins Struct Funct Bioinf 78(7):1807–1810

Motáčková V, Nováček J, Zawadzka-Kazimierczuk A, Kazimierczuk K, Žídek L, Koźmiński W, Sklenář V (2010) Strategy for complete NMR assignment of disordered proteins with highly repetitive sequences based on resolution-enhanced 5D experiments. J Biomol NMR 48(3):169–177

Mukrasch M, Bibow S, Korukottu J, Jeganathan S, Biernat J, Griesinger C, Mandelkow E, Zweckstetter M (2009) Structural polymorphism of 441-residue Tau at single sesidue resolution. PLoS Biol 7(2):399–414

Narayanan RL, Durr UHN, Bibow S, Biernat J, Mandelkow E3, Zweckstetter M (2010) Automatic assignment of the intrinsically disordered protein tau with 441-residues. J Am Chem Soc 132(34):11906–11907

Orekhov VY, Ibraghimov IV, Billeter M (2001) MUNIN: a new approach to multi-dimensional NMR spectra interpretation. J Biomol NMR 20(1):49–60

Panchal SC, Bhavesh NS, Hosur RV (2001) Improved 3D triple resonance experiments, HNN and HN(C)N, for H-N and N-15 sequential correlations in (C-13, N-15) labeled proteins: application to unfolded proteins. J Biomol NMR 20(2):135–147

Pannetier N, Houben K, Blanchard L, Marion D (2007) Optimized 3D-NMR sampling for resonance assignment of partially unfolded proteins. J Magn Reson 186(1):142–149

Perez Y, Gairi M, Pons M, Bernado P (2009) Structural characterization of the natively unfolded N-terminal domain of human c-Src kinase: insights into the role of phosphorylation of the unique domain. J Mol Biol 391(1):136–148

Pervushin K, Vogeli B, Eletsky A (2002) Longitudinal H-1 relaxation optimization in TROSY NMR spectroscopy. J Am Chem Soc 124(43):12898–12902

Peti W, Smith LJ, Redfield C, Schwalbe H (2001) Chemical shifts in denatured proteins: resonance assignments for denatured ubiquitin and comparisons with other denatured proteins. J Biomol NMR 19(2):153–165

Rovnyak D, Frueh DP, Sastry M, Sun ZYJ, Stern AS, Hoch JC, Wagner G (2004) Accelerated acquisition of high resolution triple-resonance spectra using non-uniform sampling and maximum entropy reconstruction. J Magn Reson 170(1):15–21

Sattler M, Schleucher J, Griesinger C (1999) Heteronuclear multidimensional NMR experiments for the structure determination of proteins in solution employing pulsed field gradients. Prog Nucl Mang Reson Spect 34(2):93–158

Schanda P, Brutscher B (2005) Very fast two-dimensional NMR spectroscopy for real-time investigation of dynamic events in proteins on the time scale of seconds. J Am Chem Soc 127(22): 8014–8015

Seepersaud R, Needham RHV, Kim CS, Jones AL (2006) Abundance of the δ subunit of RNA polymerase is linked to the virulence of *Streptococcus agalactiae*. J Bacteriol 188(8):2096–2105

Sklenář V (1995) Suppression of radiation damping in multidimensional NMR experiments using magentic-field gradients. J Magn Reson Ser A 114(1):132–135

Sørensen OW, Eich GW, Levitt MH, Bodenhausen G, Ernst RR (1984) Product operator formalism for the description of NMR pulse experiments. Prog Nucl Mang Reson Spect 16:163–192

Stern AS, Li KB, Hoch JC (2002) Modern spectrum analysis in multidimensional NMR spectroscopy: comparison of linear-prediction extrapolation and maximum-entropy reconstruction. J Am Chem Soc 124(9):1982–1993

Sun ZYJ, Frueh DP, Selenko P, Hoch JC, Wagner G (2005) Fast assignment of N-15-HSQC peaks using high-resolution 3D HNcocaNH experiments with non-uniform sampling. J Biomol NMR 33(1):43–50

Ward JJ, Sodhi JS, McGuffin LJ, Buxton BF, Jones DT (2004) Prediction and functional analysis of native disorder in proteins from the three kingdoms of life. J Mol Biol 337(3):635–645

Yao J, Chung J, Eliezer D, Wright PE, Dyson HJ (2001) NMR structural and dynamic characterization of the acid-unfolded state of apomyoglobin provides insights into the early events in protein folding. Biochemistry 40(12):3561–3571

Zawadzka-Kazimierczuk A, Kazimierczuk K, Koźmiński W (2010) A set of 4D NMR experiments of enhanced resolution for easy resonance assignment in proteins. J Magn Reson 202(1):109–116

Zweckstetter M, Bax A (2001) Single-step determination of protein substructures using dipolar couplings: aid to structural genomics. J Am Chem Soc 123(39):9490–9491